optica

Serpentine optical phased arrays for scalable integrated photonic lidar beam steering

Nathan Dostart,[1,†,*] Bohan Zhang,[2,†] Anatol Khilo,[2,3] Michael Brand,[1] Kenaish Al Qubaisi,[2] Deniz Onural,[2] Daniel Feldkhun,[1] Kelvin H. Wagner,[1] and Miloš A. Popović[2]

[1]Department of Electrical, Computer, and Energy Engineering, University of Colorado, Boulder, Colorado 80309, USA
[2]Department of Electrical and Computer Engineering, Boston University, Boston, Massachusetts 02215, USA
[3]Currently at: Ayar Labs, 6460 Hollis St, Ste A, Emeryville, California 94608, USA
*Corresponding author: nathan.dostart@colorado.edu

Received 18 February 2020; revised 4 May 2020; accepted 15 May 2020 (Doc. ID 389006); published 17 June 2020

Optical phased arrays (OPAs) implemented in integrated photonic circuits could enable a variety of 3D sensing, imaging, illumination, and ranging applications, and their convergence in new lidar technology. However, current integrated OPA approaches do not scale—in control complexity, power consumption, or optical efficiency—to the large aperture sizes needed to support medium- to long-range lidar. We present the serpentine OPA (SOPA), a new OPA concept that addresses these fundamental challenges and enables architectures that scale up to large apertures. The SOPA is based on a serially interconnected array of low-loss grating waveguides and supports fully passive, 2D wavelength-controlled beam steering. A fundamentally space-efficient design that folds the feed network into the aperture also enables scalable tiling of SOPAs into large apertures with a high fill-factor. We experimentally demonstrate, to the best of our knowledge, the first SOPA using a 1450–1650 nm wavelength sweep to produce 16,500 addressable spots in a 27 × 610 array. We also demonstrate, for the first time, far-field interference of beams from two separate OPAs on a single silicon photonic chip, as an initial step towards long-range computational imaging lidar based on novel active aperture synthesis schemes.

https://doi.org/10.1364/OPTICA.389006

1. INTRODUCTION

Optical phased arrays (OPAs) implemented in integrated photonics [1–21] can form and electronically steer free-space optical beams to be emitted from, or received by, an on-chip aperture. With the prospect of integration in CMOS platforms to form small-sized, low-power, and low-cost electronic–photonic systems-on-chip, integrated OPAs may become the enabling component for a new generation of photonic sensing technologies. Furthermore, if they could scale to larger, centimeter-, reticle- or even wafer-scale apertures, silicon OPAs could make obsolete many bulk optic [22,23] and semi-integrated [24–30] approaches while enabling new, revolutionary imaging modalities [31].

General OPA designs, capable of forming arbitrary far-field patterns, may rely on 2D arrays of antenna elements [2,4,12,13] fed via independently controlled phase shifters. They can cohere to form a single steering beam, but such approaches require an $N \times N$ array of phase shifters, each dissipating power and requiring rapid individual control, to address N^2 spots. When the far-field pattern of interest is one or more steered beams, a reduced control complexity is enabled by a hybrid 1D phase shifter plus 1D wavelength beam steering using an array of parallel 1D grating waveguides [3,5,6,9–11,14,16]. This approach takes advantage of the natural angular dispersion of grating couplers to steer the beam in one dimension with wavelength, thereby reducing the number of required phase shifters from approximately N^2 to N. These 1 + 1D OPA designs therefore use wavelength as a degree of freedom to decrease control complexity and power consumption. In addition to the remaining phase shifters, 1 + 1D designs demonstrated to date inherently allocate one to two orders of magnitude larger optical frequency bandwidth per spot (60–100 GHz) than that needed for lidar ranging (1–10 GHz). This translates to a sparsely populated optical spectrum, making inefficient use of wavelength as a control parameter, and opens the door to increased noise from amplified spontaneous emission as well as a power inefficiency, since the optical spectrum is contiguously generated.

Current OPA approaches have, including for some of the foregoing reasons, been limited from scaling to large (1 cm^2 and larger) apertures that are necessary for high-performance lidar. Implementing such apertures using current approaches would require, at minimum, thousands of phase-modulating elements rapidly and precisely controlled to form continuously steering beams. The associated control complexity and power dissipation has been a significant factor in limiting achievable aperture size. Additional factors that limit aperture size are waveguide propagation loss, and the characteristic length scales of phase error accumulation across the aperture.

Construction of a large aperture as a tiled array of smaller sub-aperture tiles could take advantage of hierarchical control schemes and efficiently address some of the issues limiting aperture size. In a suitable choice of tile and array configuration, only one phase shifter may be needed per OPA tile to both enable steering of the tiled aperture and correct for phase errors between OPAs. However, the tiling approach can have low optical efficiency and additional beam sidelobes for apertures with low fill-factors, i.e., where substantial area is used by power feed structures and other non-emitting components. The latter is a persistent issue for 1 + 1D demonstrations to date.

In this paper, we introduce the serpentine OPA (SOPA), a new passive and simple-to-control OPA concept designed to address these fundamental challenges and enable large-scale tiled-array apertures. The SOPA uses a delay-accumulating, serpentine waveguide structure to wavelength-steer beams in two dimensions. The passive serpentine structure—enabled by ultra-low-loss waveguides, tapers, and single-mode bends—steers the beam along the two orthogonal angular directions via respective coarse (here, 40 GHz) and fine (1.5 GHz) frequency shifts. It nominally requires no active phase shifters. It also fully utilizes the optical spectrum. The SOPA matches the ranging bandwidth to the fine beam-steering frequency increment and completely populates the utilized optical spectrum without gaps. The 2D wavelength-steered approach thereby reduces N^2 degrees of freedom to just one (per beam), the optical wavelength, while using the wavelength spectrum with maximum efficiency. It allows multiple beams to be simultaneously emitted or received by simply addressing multiple wavelengths. The SOPA additionally uses interstitial flyback waveguides to accumulate delay across the aperture and incorporate the feed network into the OPA itself, thus allowing near unity fill-factors appropriate for tiled apertures. The increased resolution and power provided by larger lidar apertures can be realized by transmitting from an array of SOPA tiles that interfere on a target. Tiling is also compatible with computational imaging techniques [31] that can correct for unknown tile phases using only the back-scattered detected signal, alleviating phase-cohering requirements. We demonstrate the SOPA concept through 2D beam steering experiments showing 16,500 addressable spots, and the tiling approach through far-field interference of beams emitted by two SOPA tiles on a single chip. These results present a first step toward low-complexity OPAs with tractable scaling to large synthetic apertures.

2. SERPENTINE OPTICAL PHASED ARRAY

The SOPA produces 2D optical beam steering by using an aperture-integrated delay-line "feed network" that in principle requires zero power and nearly zero excess footprint. It is this feature that makes the SOPA extraordinarily easy to operate and suitable to be tiled into large arrays.

An integrated OPA consists of a 2D array of radiating elements with a feed network that distributes optical power to the elements and controls the phase of their emission for beam forming and steering. The architecture of the feed network determines the OPA's control complexity, footprint, and ultimately its scalability. Purely electronic phase control, where every radiating element is preceded by an independently controllable phase shifter [2], requires large numbers of phase shifters. Frequency-based phase control uses dispersive grating couplers, delay lines, or both to map the wavelength to a beam emission angle according to a frequency-dependent phase (time delay), which avoids phase shifters entirely but "hard-wires" the steering control to the OPA design. Most OPAs demonstrated to date have used purely electronic steering [2,4,12,13] or replaced one dimension of steering control with wavelength by using an array of waveguide gratings, each fed by a split and phase-shifted copy of the input signal [3,5–11,14–17,32,33]. However, the presence of electronically controlled phase shifters within the OPA rapidly increases the OPA's complexity as it increases in size, making centimeter-scale apertures difficult to control.

The key to the SOPA concept is to steer with wavelength in both dimensions by using grating couplers in one dimension and a sequential folded serpentine delay line in the other. This allows the frequency of a single tunable laser to control the entire OPA, eliminating the need for phase shifters entirely. To make the SOPA as simple and space efficient as possible, the gratings (red) are incorporated directly into the delay line by means of a serpentine structure (blue) (Fig. 1a). Thus, unlike the initial 2D wavelength-steered OPA approach that used delay lines external to the gratings [1], the SOPA's delay line feed network incurs near zero area overhead and is independent of aperture size. We also show that the SOPA demonstrates improved performance compared to the previous 2D wavelength-steered OPA [1]: a 400× larger aperture and 300× more spots, enabling performance comparable to the state of the art. This is achieved through development of ultra-low-loss components in this work and optimal use of the frequency domain (each addressable spot takes up only as much bandwidth as needed for the desired ranging resolution). By removing the need for phase shifters, and efficiently using wavelength as an easily accessible control parameter, many SOPA devices can be arrayed on a single chip to create centimeter-scale apertures that drastically outperform other OPA approaches.

The serpentine delay structure steers beams in two orthogonal dimensions by tuning the wavelength/frequency in respectively coarse and fine increments, as illustrated in Figs. 1(b) and 1(c), analogous to a falling raster [34] demonstrated previously with dispersive reflectors in a free-space configuration [35].

The SOPA's beam steering capability is best understood in terms of the frequency resolvability of the array, which relates the time delay across the aperture to the frequency shift required to steer by one spot. The delay accumulated along a single grating waveguide (τ) is exactly the inverse of the frequency step ($\Delta f = 1/\tau$) required to steer the beam by one resolvable spot along the grating-waveguide dimension θ_x [Fig. 1(d)]. The delay accumulated across the M serpentine rows of the aperture can be defined as $T = MC\tau$, where C is a scaling factor that denotes the ratio of time delay accumulated between rows relative to the single-pass time delay through a grating [$C = (\tau + \tau_{\text{flyback}} + 2\tau_{\text{bend}} + 4\tau_{\text{taper}})/\tau$]. For an ideal 2D SOPA raster, $C = 1$. The increased delay across all M rows relative to the delay within a grating therefore results in a "finer" (smaller) frequency step to steer by one resolvable spot along θ_y [Fig. 1(e)] than the "coarse" (large) step needed to steer along θ_x. This arrangement causes the beam to steer quickly along θ_y and slowly along θ_x for a linear ramp of the optical frequency. The slow scan along θ_x combined with the periodic resetting of the steering angle along θ_y as the row-to-row phase increments by 2π results in a 2D raster scan of the field of view (FOV) controlled entirely by the frequency/wavelength.

A mathematical model for 2D beam steering with frequency is obtained by considering the SOPA as a phased array. Along x,

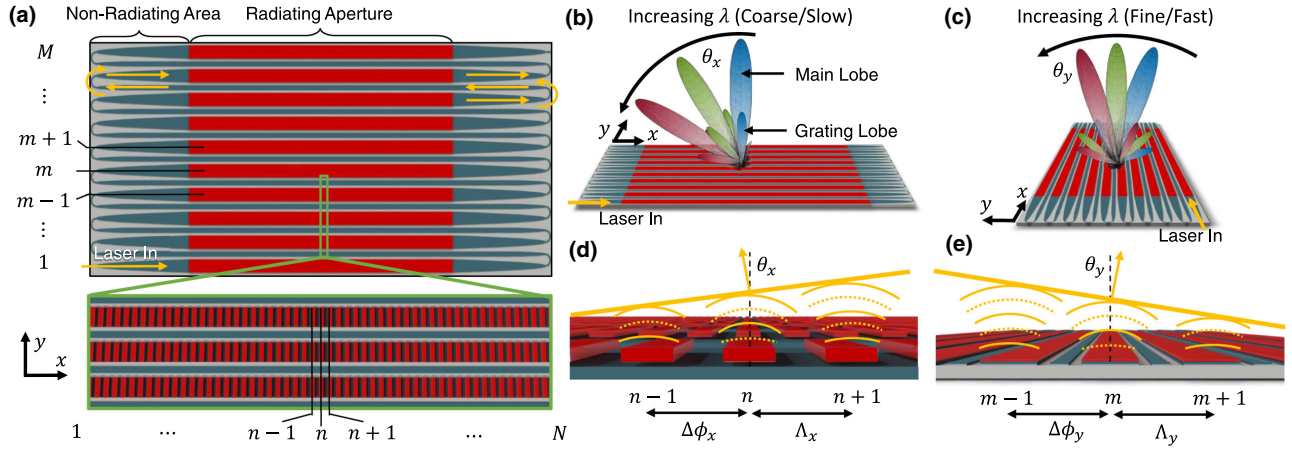

Fig. 1. Serpentine optical phased array 2D wavelength steering. (a) Schematic of SOPA tile topology. An array of M rows of grating waveguides (red) are serially connected by flybacks (blue) in a serpentine configuration. Each row has N grating periods. (b) Coarse (slow) wavelength steering. (c) Fine (fast) wavelength steering. (d) For coarse steering along θ_x, each grating waveguide diffracts light to an angle determined by the wavelength-dependent tooth-to-tooth phase delay. (e) For fine steering along θ_y, the array of gratings diffracts light to an angle determined by the wavelength-dependent row-to-row phase delay.

light is coupled out at an angle $\theta_x(f)$ through a phase matching condition:

$$\theta_x(f) = \sin^{-1}\left(\frac{c}{2\pi f}\left[\frac{\Delta\phi_x(f)}{\Lambda_x} + q\frac{2\pi}{\Lambda_x}\right]\right), \quad q \in \mathcal{Z}$$

$$= \sin^{-1}\left(n_{\text{eff}}(f) - \frac{c}{f\Lambda_x}\right), \tag{1}$$

where Λ_x is the grating period, n_{eff} is the effective index of the waveguide mode, q is the diffraction order, and $\Delta\phi_x(f)$ is the relative phase between grating periods and is given by $\Delta\phi_x(f) = 2\pi f n_{\text{eff}}(f)\Lambda_x/c$. We choose the grating period so that only the first diffraction order, $q = -1$, is radiating.

The diffraction angle along y, $\theta_y(f)$, is given by

$$\theta_y(f) = \sin^{-1}\left(\frac{c}{f\Lambda_y}\frac{\text{mod}_{2\pi}\left[\Delta\phi_y(f)\right]}{2\pi}\right), \tag{2}$$

where Λ_y is the row-to-row pitch, $\Delta\phi_y(f)$ is the differential phase between adjacent grating waveguides (equal to the phase accumulated across the preceding grating waveguide and additional connecting components), and $\text{mod}_{2\pi}[x]$ denotes the wrapped phase evaluated on the interval $(-\pi, \pi]$.

The frequency shift to steer the beam by one spot width can be found by taking the derivative of the differential phase $\Delta\phi(f)$ with respect to frequency and calculating the frequency step Δf to create a 2π phase shift across the length of the aperture: $\Delta f_i = 2\pi(\Lambda_i/L_i)(\partial\Delta\phi_i/\partial f)^{-1}$. The frequency shifts that steer the beam by one spot width along x and y, respectively, are

$$\Delta f_x = 2\pi\left(N\frac{\partial\Delta\phi_x}{\partial f}\right)^{-1} = \frac{c}{n_g(f)N\Lambda_x}, \tag{3}$$

$$\Delta f_y = 2\pi\left(M\frac{\partial\Delta\phi_y}{\partial f}\right)^{-1} = \frac{\Delta f_x}{MC}, \tag{4}$$

where n_g is the group index of the grating-waveguide mode, N is the number of periods along a single grating waveguide, M is the number of grating-waveguide rows, and C is the multiplicative constant introduced previously. It is clear from Eqs. (3) and (4) that for a coarse frequency shift of Δf_x, the beam is steered by one spot width in θ_x and by MC spot widths in θ_y, during which C is the number of times θ_y scans the y-dimension FOV.

3. SILICON PHOTONIC SOPA IMPLEMENTATION

The first implementation of the SOPA was fabricated in a silicon-on-insulator platform, shown with its components in Fig. 2. An image of the full SOPA is depicted in Fig. 2(a) where the radiating aperture can be seen as the darker pink and is captured in the IR near-field image in Fig. 2(b). The magnified image in Fig. 2(c) also contains labels for the single-mode adiabatic bends [Fig. 2(d)] and grating waveguides and flybacks [Fig. 2(e)].

The principal component of the SOPA, the grating waveguide, is highlighted in Fig. 2(f), with the two grating variants shown in Figs. 2(g) and 2(h). The first weakly scattering grating design uses an upper level of silicon nitride bars placed over the silicon waveguide as teeth [Figs. 2(f) and 2(g)], while the second uses rectangular corrugations on the sidewalls of the silicon waveguide [Fig. 2(h)]. In this SOPA implementation, the gratings were designed to radiate normal to the plane of the chip at a wavelength of approximately 1300 nm (460 nm grating period).

The SOPA's serially connected grating delay-line geometry represents the key design challenge for this approach: for long optical path lengths, weak gratings and low routing losses are needed. For the results shown in this paper, the geometric optical path length is 6.4 cm with 128 tapers and 64 bends. One of the dominant sources of on-chip waveguide propagation losses is scattering due to line edge roughness. We designed wide (6.5 μm) waveguides that exceed the single-mode width (500 nm) to mitigate this loss, similar to [36]. Parabolic tapers are used to transition from wide waveguides to single-mode width inter-row U-bends without exciting higher-order modes. The inter-row U-bends are designed for ultra-low insertion loss by employing an adiabatically varying curvature [37,38] that minimizes bend loss without junction losses. The predicted and measured component losses are shown in Fig. 2(j).

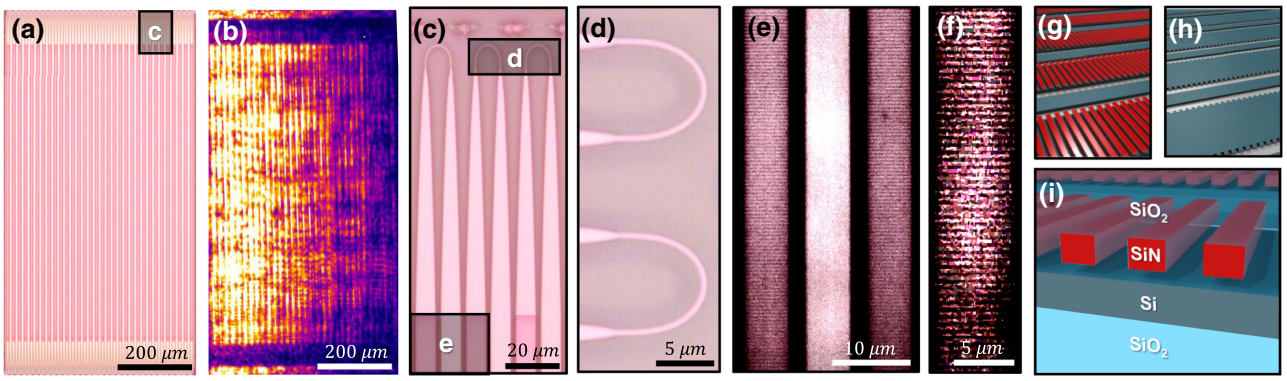

(j)

Component	Design Loss	Measured Loss	Used in SOPA	Total Measured Loss	Expected Loss (Next Gen)	Total Loss (Next Gen)
Bend	0.001 dB	0.003 dB	64 units	0.2 dB	0.003 dB	0.2 dB
Taper	0.05 dB	0.07 dB	128 units	9 dB	0.004 dB	0.5 dB
Waveguide	-	0.06 dB/cm	6.4 cm	0.4 dB	0.06 dB/cm	0.4 dB

Fig. 2. Images of fabricated SOPA emission pattern and components. (a) Optical micrograph of the fabricated SOPA where the radiating aperture is darker pink. (b) Near-field IR image of the SOPA emission, showing emission decay across the aperture resulting primarily from taper losses. (c) Zoomed view of all SOPA components, centered on the parabolic tapers, with labels for the single-mode adiabatic bends and waveguides. (d) Single-mode adiabatic bends. (e) Two grating waveguides (left and right) and a single flyback waveguide (center). (f) High magnification image of the nitride bar grating. (g) Rendering of a SOPA with nitride bar grating variant. (h) Rendering of a SOPA with silicon sidewall grating variant. (i) Fabrication cross section of the nitride bar grating. (j) SOPA loss budget.

In this SOPA implementation, each SOPA tile is ∼1 mm × 0.5 mm in size with a radiating aperture of ∼0.8 mm × 0.5 mm, which results in 82% of the footprint occupied by the radiating aperture. The length of each grating-waveguide row is 0.8 mm, and the remaining ∼0.2 mm is taken up by the adiabatic bends and tapers. The row-to-row pitch, Λ_y, is 16 μm, and there are 32 rows of grating waveguides and flybacks for a total tile height of 0.5 mm. The row-to-row exponential decay of the radiation visible in Fig. 2(b) is the result of a uniform loss of 9.6 dB across the aperture. This loss was dominated by the tapers, contributing 9 dB of the measured 9.6 dB total loss across the aperture. This decay can be addressed by both lower loss components and grating strength, which increases across the SOPA (grating apodization) such as in Refs. [11,32]. The SOPA design presented here utilized parabolic tapers, resulting in relatively high loss. By utilizing adiabatic taper designs with a Hamming window coupling distribution in the next generation of SOPAs [39], we expect to reduce taper losses from 9 dB to 0.5 dB and thereby reduce the total excess loss across the aperture from 9.6 dB to 1.1 dB. Based on this geometry, we estimate coarse and fine frequency steps, respectively, of $\Delta f_x \approx 80$ GHz and $\Delta f_y \approx 1$ GHz from Eqs. (3) and (4), where a factor of $C = 2.4$ can be assumed using the geometric length of the SOPA structure.

4. SINGLE-TILE BEAM FORMING EXPERIMENTS

To demonstrate the low-complexity beam steering required for scaling to large apertures, we characterize the spot size, FOV, number of addressable spots, and scan rates of a single SOPA tile. Experimental results at 1550 nm of the far-field emission pattern of a single SOPA tile using the nitride bar design are shown in Fig. 3. This SOPA implementation forms a collimated rectangular beam at the chip surface, with Rayleigh range of approximately 43 cm for the transverse profile along the x axis and 17 cm along the y axis. We measure a full-width at half-maximum (FWHM) spot size of $\Delta\theta_x = 0.11°$ by $\Delta\theta_y = 0.2°$, close to the diffraction-limited size of 0.1° by 0.16°, without any active phase tuning. Enlarged side lobes are visible adjacent to the main lobe along θ_y in Figs. 3(b) and 3(c) (side mode suppression ratio of ∼3 dB) due predominantly to row-to-row phase errors accumulated along the 6.4 cm path length. These phase errors will require further reduction or compensation in subsequent SOPA designs. For OPAs with element pitches greater than $\lambda/2$, multiple lobes (commonly referred to as grating lobes) are emitted into the far field and thereby limit the FOV of the OPA. These grating lobes are seen at ±5.5° along θ_y in Fig. 3(a), limiting the FOV to 5.5° in this direction. Decreasing the row-to-row pitch will widen the unambiguous FOV.

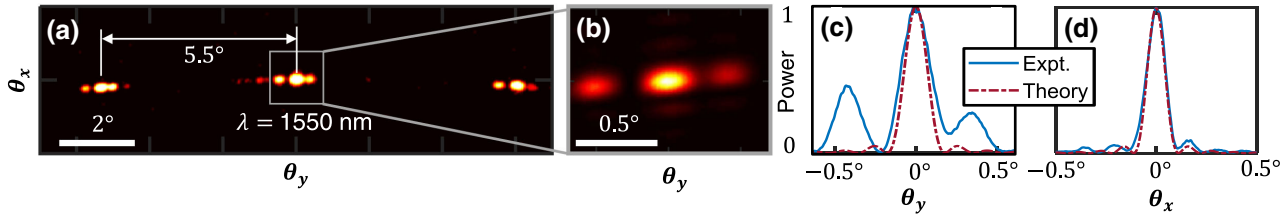

Fig. 3. Measurement results of single-tile emission pattern. (a) Example far-field emission pattern of a single tile at one wavelength showing 5.5° grating lobe spacing. (b) Zoomed image of the main lobe. (c) Cross section along θ_y of the main lobe with measured full-width half-max (FWHM) of 0.2° and side lobes. (d) Cross section along θ_x of the main lobe with measured FWHM of 0.11°.

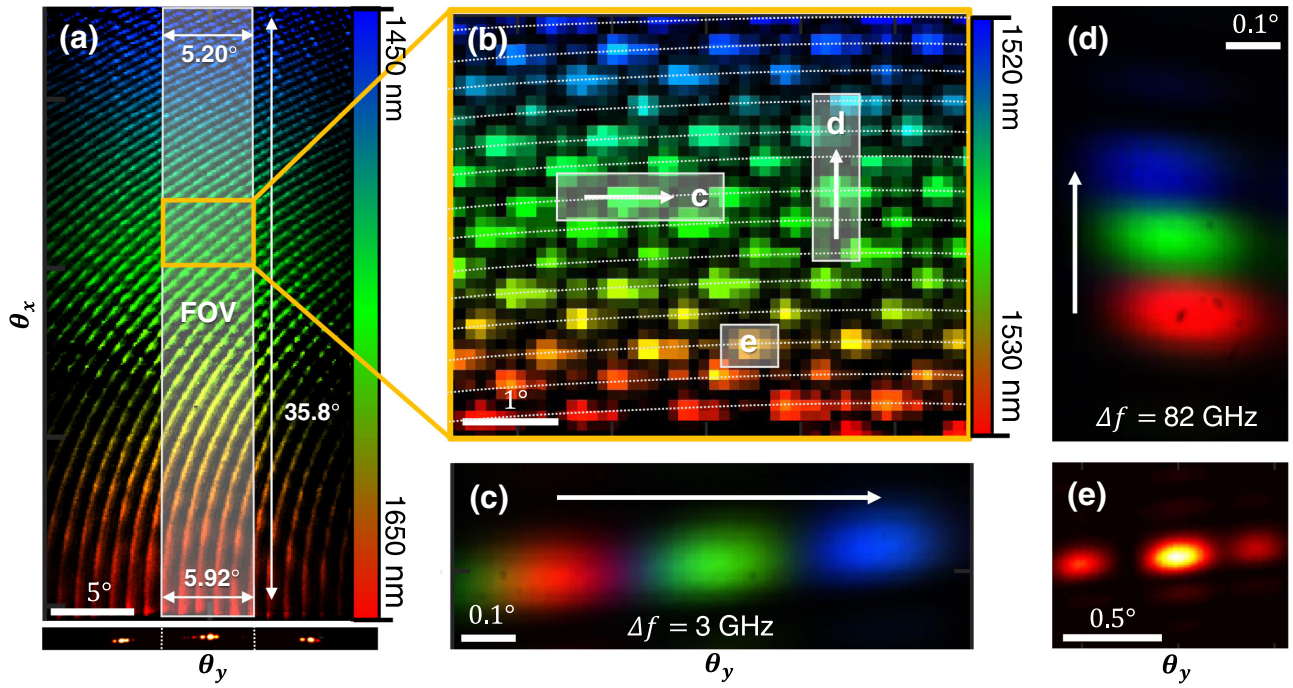

Fig. 4. Demonstration of 2D wavelength steering with a SOPA. (a) Far-field camera image of a 200 nm scan (see Visualization 1), with only 1500 spots sampled out of 16,500. The grating lobe-limited FOV is 35.8° × 5.5°. The under-sampling of the scan (every 10th point) and saturated over-exposure applied in post-processing for visibility cause the appearance of diagonal curves that are not the actual scan loci; their curvature arises from the group velocity dispersion. The spot pattern at 1550 nm is shown at the bottom to demonstrate the grating lobe-limited FOV. (b) A 5° × 5.5° subsection of the full scan, with only 70 spots sampled. The true scan loci are depicted by the dotted lines as a guide to the eye, and the colors are re-coded for the narrower bandwidth. (c) Wavelength scanning along the fast axis with three non-adjacent spots spaced by 3 GHz. (d) Wavelength scanning along the slow axis with three non-adjacent spots spaced by 82 GHz. (e) Single-wavelength spot at 1550 nm.

Beam steering results are shown in Fig. 4 demonstrating both a full 200 nm wavelength sweep as well as scanning rates along both dimensions (see Visualization 1). We measure a $\Delta f_x = 41.3$ GHz frequency shift to steer to the next addressable spot along θ_x (82.6 GHz to the next fully resolvable spot) and a $\Delta f_y = 1.53$ GHz frequency shift to steer to the next resolvable spot along θ_y. We measured 27 FWHM resolvable spots along θ_y (out of 32 at the diffraction limit) and 610 addressable spots along θ_x for a total of 16,470 addressable spots (see Supplement 1 for measurements of resolvability and further discussion). Total insertion loss from the laser into the main lobe of the emission pattern varies between 10 dB and 30 dB across different SOPA grating design variants, and we measured an approximately 30 dB insertion loss for the grating variant used for Figs. 3 and 4. Future improvements to the SOPA should reduce this to under 6 dB by reducing taper losses and by using the higher efficiency gratings adjusted to better match the SOPA size.

5. SCALING UP APERTURE SIZE BY TILING

In order to increase the aperture size beyond a single tile we use an array of SOPA tiles to interferometrically form a composite aperture [31]. The tiling approach provides a means to create a larger effective aperture than is feasible with a single contiguous OPA tile with a scheme that can be extended to arbitrarily large aperture sizes. For example, our fabricated test aperture shown in Fig. 5(a) is approximately 20 mm^2, much larger than can be achieved with a single SOPA tile (0.5 mm^2) that could be limited in size by waveguide loss, phase error accumulation, and, for lidar applications, ranging bandwidth.

The tiling approach is conceptually simple: an array of identical OPAs is fed in parallel by a distribution network (e.g., splitter tree) with a single input laser, and each OPA is preceded by a single phase shifter to facilitate array-level beam steering. All OPAs, emitting simultaneously, beam steer to the same far-field spot to create overlapping and coherently interfering spots on the target. This beam alignment of multiple OPAs is automatic for 2D wavelength-steered OPAs, such as the SOPA, when driven by a common laser; phase-shifter steered OPAs require additional control to ensure beam alignment. When all tiles emit with identical phase, a smaller "array" spot is formed in the center of the overlapping "tile" spots. Linear phase ramps applied (via the array-level phase shifters) across the array of tiles along x and y will steer the array spot in 2D within the bounds of the tile spot, enabling imaging within the tile spot. The array of tiles thereby creates a larger effective aperture composed of individual OPAs, the tiled aperture, achieving correspondingly higher overall tiled-aperture resolution.

One potential downside of the tiling approach is the creation of additional radiation lobes ("tiling lobes"), which are directly analogous to the grating lobes produced by the gaps in element spacing in OPAs [2,12]. These tiling lobes affect system performance by diverting transmitted (or received) power away from the main lobe, which decreases the signal-to-noise ratio (SNR) and introduces ambiguity to a lidar or imaging system. These effects are minimized when the separation between radiating elements of adjacent tiles is minimized, which can be quantified by a "tiling fill-factor" (TFF) metric we introduce as

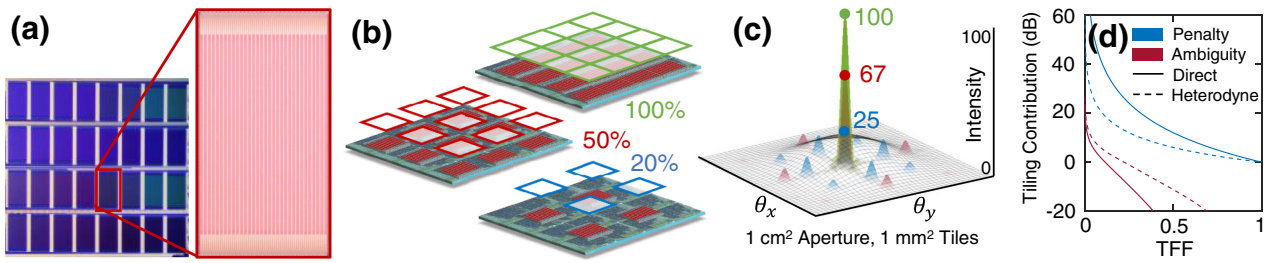

Fig. 5. Beam steering with tiled apertures. (a) Image of the fabricated SOPA tiled aperture. (b) Illustration of tiled apertures with varying tiling fill-factor (TFF). (c) Radiation patterns of tiled apertures with TFFs from (b) relative to a single tile (20× magnified). (d) Relation of TFF to the contribution of tiling lobes to SNR penalty and ambiguity for both direct detection and heterodyne detection.

$$\mathrm{TFF} \equiv \frac{\text{area of emitting sub-aperture}}{\text{total tile area}}. \tag{5}$$

The TFF should not be confused with the fill-factor of the OPA tile's radiating aperture, a separate metric that captures the density of radiating elements within a single OPA tile and correspondingly correlates with the power radiated into grating lobes. The product of the TFF and the OPA tile's fill-factor captures the combined effects of both tiling and grating lobes.

The TFF correlates directly with the aforementioned effects of decreased SNR and increased ambiguity, as shown in Figs. 5(b)–5(d) for a lidar system using identical tiled apertures for both the transmitter and receiver. For an OPA composed of rectangular apertures and direct detection, the "tiling penalty" to SNR scales proportionally to $1/\mathrm{TFF}^4$. Defining the ambiguity of the measurement as the ratio of erroneous signal (due to tiling lobes) to actual signal (due to the main lobe), the same system has a "tiling ambiguity" proportional to $1/\mathrm{TFF}$ for low TFF. It is therefore essential to use OPA designs with high TFF when using the tiled-aperture approach.

6. TWO-TILE APERTURE SYNTHESIS EXPERIMENTS

We demonstrate the creation of a larger effective aperture using the tiled-aperture approach by transmitting simultaneously from two SOPA tiles (Fig. 6). These results constitute, to the best of our knowledge, the first demonstration of tiled-aperture optical beam steering.

The tiles are located on the same chip with center-to-center separation of 2.3 mm, as shown in Fig. 6(a). The measured far-field fringe pattern is shown in Fig. 6(b) and demonstrates phase uniformity within the far-field spot, an essential ingredient for aperture synthesis. Figure 6(c) depicts shifting of the fringe pattern as the input phase to one of the tiles is changed, demonstrating the phase control necessary for both diffraction-limited tiled-aperture beam forming and "super-resolved" structured illumination imaging within a single far-field spot [31]. Although we use off-chip phase control for these initial experiments, future designs will include active integrated phase shifters for this purpose. An additional requirement for tiled-aperture operation is that every tile steers to the same far-field spot, which we demonstrate with our two tiles in Figs. 6(d) and 6(e). As the beams steer, the fringe visibility remains high, indicating that the beams remain coherent and power-balanced as the wavelength is tuned. The experiments were restricted to using two of the 32 tiles comprising the array in this first demonstration because the array is composed of matching pairs of 16 different tile design variants (each having a different radiator grating design or variation). Two-tile experiments suffice to provide the information relevant to tiled-aperture operation.

7. DISCUSSION

To demonstrate the SOPA's scalability to larger apertures via tiling, its performance is compared to selected results from the literature in Table 1, both as a standalone aperture and when multiple tiles are combined to form a 1 cm^2-sized tiled aperture as needed for

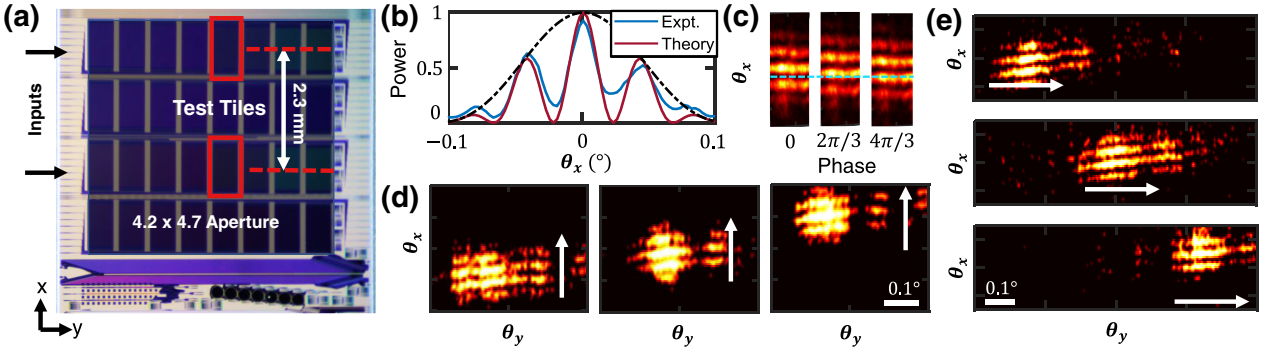

Fig. 6. Demonstration of tiled-aperture operation. (a) Test chip showing 4.2 × 4.7 mm^2 tiled aperture with the tiles used for the interference demonstration highlighted. (b) Comparison of expected and measured fringe visibility demonstrating beam balance and tile coherence. (c) Demonstration of relative phase-shift control (see Supplement 1, Sec. 3) between tiles with visible phase shift asymmetry about the dotted line. (d) Same-angle wavelength steering of both tiles in the slow scanning direction ($\Delta f = 82$ GHz steps). (e) Same-angle wavelength steering of both tiles in the fast scanning direction ($\Delta f = 3$ GHz steps).

Table 1. Performance Comparison of Demonstrated 2D Integrated Beam Steering Apertures

Steering Method	[2]	[12]	[3]	[5]	[6]	[16]	[10]	[1]	This Work
	2D Phase Shifter		*1D Wavelength, 1D Phase Shifter*					*2D Wavelength*	
Single-Aperture Performance									
Phase shifters	64	128	16	32	128	512	32	0	0
Radiating area (mm^2)	0.0052	0.023	0.0048	0.032	0.49[a]	10	1.3	0.001[a]	0.4
Spots	64	400	500	140	60,000	190,000[a]	45,000	50	16,500
FOV (°)	6.0 × 6.0	16 × 16	20 × 15	23 × 3.6	80 × 17	15 × 56	28 × 22	15 × 50	36 × 5.5
1 cm^2 Tiled-Aperture Extrapolated Performance									
Tiling fill-factor	0.11[b]	0.18[b]	0.003[a]	0.005[a]	0.083[a]	0.70[a]	0.31[a]	0.2[a]	**0.82**
Phase shifters	1,300,000	570,000	1100[a]	500[a]	2100[a]	3600[a]	790[a]	20,000[a]	**200**

[a]Value estimated from figures or other stated parameters.
[b]2D phase-shifter tiles have TFF identical to the tile internal fill-factor.

moderate-range (~100 m) lidar. The TFF of 82% in this initial demonstration and use of 2D wavelength steering at the single-tile level lead to high-density tiling and far fewer phase shifters than competing approaches at the tiled-aperture level. A 1 cm^2 SOPA tiled aperture using the initial SOPA tile design in this paper requires only 200 phase shifters, one per tile. By comparison, approaches using phase-shifter steering generally require large numbers of phase shifters (>1000) or have degraded performance due to low TFF (<10%). Only two recent designs [10,16] have both a high TFF and manageable number of phase shifters at the centimeter-aperture scale.

Achieving the full potential of the SOPA architecture requires a suitable laser source—large tuning range, rapid tuning, excellent frequency stability, accurate wavelength calibration, and mode hop-free tuning. Tunable integrated lasers have demonstrated in excess of 50 nm sweep ranges, and some demonstrations such as Ref. [40] operate without mode hopping. SOPA beam steering using the hybrid silicon laser in Ref. [40] would therefore achieve approximately 4000 spots and would not require additional calibration.

As a standalone aperture, the SOPA excels in its minimal electronic complexity, while achieving aperture size, number of spots, and FOV comparable to the state of the art. Several improvements have been made to the SOPA design for increased performance in future generations. Interleaving SOPAs, each addressing a half-space, allows doubling of the slow axis angular scan range to nearly 80°. The FOV along the fast dimension has been widened to 18° by reducing the row-to-row pitch down to 5 μm and optimizing for low waveguide, taper, and bending loss. Designs with shortened tapers achieved upwards of 92% TFF. Improvements to spot quality, which is currently not diffraction limited due to fabrication non-uniformity, can be realized with only two to four thermal phase tuners integrated directly into the SOPA without reducing TFF. More efficient SOPA delay accumulation ($C \rightarrow 1$) will reduce the phase errors and may be sufficient to avoid phase-error compensation entirely. Apodized and multi-level grating designs [41] will enable unidirectional emission, maximum power extraction, and improved beam profiles. Other improvements include spatial Vernier topologies for grating lobe suppression in bidirectional lidar [18] and a Fourier-basis self-calibrated tiled-aperture imaging approach [31].

In this paper, we demonstrated the SOPA silicon photonic wavelength controlled 2D beam steering tile, an OPA designed from the outset for low-complexity, large-area, tiled apertures. Our delay-accumulating serpentine waveguide design allows for compact, wavelength-steered tiles that pack efficiently into an array and do not require active control. We demonstrated a SOPA tile with nearly diffraction-limited performance, 16,500 addressable spots, wide FOV, and record tiling density, as well as interferometric beam combination with two-tile simultaneous beam steering emulating aperture synthesis imaging from a large array of SOPA tiles. We believe that the SOPA design is a promising solution for achieving easily controllable, large, 2D beam steering apertures demanded by applications such as long-range integrated photonic lidar.

Funding. U.S. Department of Defense (GS00Q14 OADS139); National Science Foundation (1144083); David and Lucile Packard Foundation (2012-38222).

Acknowledgment. The authors thank Hayk Gevorgyan for help with setting up edge-coupling to the chip. Chip layout was carried out using an academic license of Luceda Photonics IPKISS.

Disclosures. The authors declare no conflicts of interest.

See Supplement 1 for supporting content.

[†]These authors contributed equally to this work.

REFERENCES

1. K. Van Acoleyen, W. Bogaerts, and R. Baets, "Two-dimensional dispersive off-chip beam scanner fabricated on silicon-on-insulator," IEEE Photon. Technol. Lett. **23**, 1270–1272 (2011).
2. J. Sun, E. Timurdogan, A. Yaacobi, E. S. Hosseini, and M. R. Watts, "Large-scale nanophotonic phased array," Nature **493**, 195–199 (2013).
3. D. Kwong, A. Hosseini, J. Covey, Y. Zhang, X. Xu, H. Subbaraman, and R. T. Chen, "On-chip silicon optical phased array for two-dimensional beam steering," Opt. Lett. **39**, 941–944 (2014).
4. K. Sayyah, O. Efimov, P. Patterson, J. Schaffner, C. White, J.-F. Seurin, G. Xu, and A. Miglo, "Two-dimensional pseudo-random optical phased array based on tandem optical injection locking of vertical cavity surface emitting lasers," Opt. Express **23**, 19405–19416 (2015).
5. J. Hulme, J. Doylend, M. Heck, J. Peters, M. Davenport, J. Bovington, L. Coldren, and J. Bowers, "Fully integrated hybrid silicon two dimensional beam scanner," Opt. Express **23**, 5861–5874 (2015).
6. D. N. Hutchison, J. Sun, J. K. Doylend, R. Kumar, J. Heck, W. Kim, C. T. Phare, A. Feshali, and H. Rong, "High-resolution aliasing-free optical beam steering," Optica **3**, 887–890 (2016).
7. C. V. Poulton, M. J. Byrd, M. Raval, Z. Su, N. Li, E. Timurdogan, D. Coolbaugh, D. Vermeulen, and M. R. Watts, "Large-scale silicon nitride

nanophotonic phased arrays at infrared and visible wavelengths," Opt. Lett. **42**, 21–24 (2017).
8. C. V. Poulton, A. Yaacobi, D. B. Cole, M. J. Byrd, M. Raval, D. Vermeulen, and M. R. Watts, "Coherent solid-state lidar with silicon photonic optical phased arrays," Opt. Lett. **42**, 4091–4094 (2017).
9. T. Komljenovic, R. Helkey, L. Coldren, and J. E. Bowers, "Sparse aperiodic arrays for optical beam forming and lidar," Opt. Express **25**, 2511–2528 (2017).
10. W. Xie, T. Komljenovic, J. Huang, and J. Bowers, "Dense III-V/Si phase shifters for optical phased arrays," in *Asia Communications and Photonics Conference (ACP)* (IEEE, 2018), pp. 1–3.
11. M. Zadka, Y.-C. Chang, A. Mohanty, C. T. Phare, S. P. Roberts, and M. Lipson, "On-chip platform for a phased array with minimal beam divergence and wide field-of-view," Opt. Express **26**, 2528–2534 (2018).
12. R. Fatemi, A. Khachaturian, and A. Hajimiri, "Scalable optical phased array with sparse 2D aperture," in *CLEO: Science and Innovations* (Optical Society of America, 2018), paper STu4B–6.
13. S. Chung, H. Abediasl, and H. Hashemi, "A monolithically integrated large-scale optical phased array in silicon-on-insulator CMOS," IEEE J. Solid-State Circuits **53**, 275–296 (2018).
14. T. Komljenovic and P. Pintus, "On-chip calibration and control of optical phased arrays," Opt. Express **26**, 3199–3210 (2018).
15. C. V. Poulton, P. Russo, E. Timurdogan, M. Whitson, M. J. Byrd, E. Hosseini, B. Moss, Z. Su, D. Vermeulen, and M. R. Watts, "High-performance integrated optical phased arrays for chip-scale beam steering and lidar," in *CLEO: Applications and Technology* (Optical Society of America, 2018), paper ATu3R–2.
16. C. V. Poulton, M. J. Byrd, P. Russo, E. Timurdogan, M. Khandaker, D. Vermeulen, and M. R. Watts, "Long-range lidar and free-space data communication with high-performance optical phased arrays," IEEE J. Sel. Top. Quantum Electron. **25**, 1–8 (2019).
17. C. V. Poulton, P. Russo, B. Moss, M. Khandaker, M. J. Byrd, J. Tran, E. Timurdogan, D. Vermeulen, and M. R. Watts, "Small-form-factor optical phased array module for technology adoption in custom applications," in *CLEO: Applications and Technology* (Optical Society of America, 2019), paper JTh5B–6.
18. N. Dostart, M. Brand, B. Zhang, D. Feldkhun, K. Wagner, and M. A. Popović, "Vernier Si-photonic phased array transceiver for grating lobe suppression and extended field-of-view," in *CLEO: Applications and Technology* (Optical Society of America, 2019), paper AW3K-2.
19. Y. Kohno, K. Komatsu, R. Tang, Y. Ozeki, Y. Nakano, and T. Tanemura, "Ghost imaging using a large-scale silicon photonic phased array chip," Opt. Express **27**, 3817–3823 (2019).
20. Y. Zhang, Y.-C. Ling, K. Zhang, C. Gentry, D. Sadighi, G. Whaley, J. Colosimo, P. Suni, and S. B. Yoo, "Sub-wavelength-pitch silicon-photonic optical phased array for large field-of-regard coherent optical beam steering," Opt. Express **27**, 1929–1940 (2019).
21. S. A. Miller, Y.-C. Chang, C. T. Phare, M. C. Shin, M. Zadka, S. P. Roberts, B. Stern, X. Ji, A. Mohanty, O. A. J. Gordillo, and U. D. Dave, "Large-scale optical phased array using a low-power multi-pass silicon photonic platform," Optica **7**, 3–6 (2020).
22. Velodyne lidar, "Puck datasheet," (2018).
23. S. Terrab, A. M. Watson, C. Roath, J. T. Gopinath, and V. M. Bright, "Adaptive electrowetting lens-prism element," Opt. Express **23**, 25838–25845 (2015).
24. P. F. McManamon, P. J. Bos, M. J. Escuti, J. Heikenfeld, S. Serati, H. Xie, and E. A. Watson, "A review of phased array steering for narrow-band electrooptical systems," Proc. IEEE **97**, 1078–1096 (2009).
25. B. Smith, B. Hellman, A. Gin, A. Espinoza, and Y. Takashima, "Single chip lidar with discrete beam steering by digital micromirror device," Opt. Express **25**, 14732–14745 (2017).
26. H. Chen, G. Tan, Y. Huang, Y. Weng, T.-H. Choi, T.-H. Yoon, and S.-T. Wu, "A low voltage liquid crystal phase grating with switchable diffraction angles," Sci. Rep. **7**, 1–8 (2017).
27. S. Hamann, A. Ceballos, J. Landry, and O. Solgaard, "High-speed random access optical scanning using a linear MEMS phased array," Opt. Lett. **43**, 5455–5458 (2018).
28. Y. Wang, G. Zhou, X. Zhang, K. Kwon, P.-A. Blanche, N. Triesault, K.-S. Yu, and M. C. Wu, "2D broadband beamsteering with large-scale mems optical phased array," Optica **6**, 557–562 (2019).
29. O. Atalar, R. Van Laer, C. J. Sarabalis, A. H. Safavi-Naeini, and A. Arbabian, "Time-of-flight imaging based on resonant photoelastic modulation," Appl. Opt. **58**, 2235–2247 (2019).
30. Y. Jiang, S. Karpf, and B. Jalali, "Time-stretch lidar as a spectrally scanned time-of-flight ranging camera," Nat. Photonics **14**, 14–18 (2020).
31. K. H. Wagner, D. Feldkhun, B. Zhang, N. Dostart, M. Brand, and M. Popović, "Super-resolved interferometric imaging with a self-cohering Si-photonic beam-steering lidar array," in *Digital Holography and Three-Dimensional Imaging* (Optical Society of America, 2019), paper M5A–1.
32. M. Raval, C. V. Poulton, and M. R. Watts, "Unidirectional waveguide grating antennas with uniform emission for optical phased arrays," Opt. Lett. **42**, 2563–2566 (2017).
33. C. T. Phare, M. C. Shin, S. A. Miller, B. Stern, and M. Lipson, "Silicon optical phased array with high-efficiency beam formation over 180 degree field of view," arXiv preprint arXiv:1802.04624 (2018).
34. D. N. Sitter and W. T. Rhodes, "Generalization of the falling raster-folded spectrum relationship," Appl. Opt. **29**, 2527–2531 (1990).
35. T. Chan, E. Myslivets, and J. E. Ford, "2-Dimensional beamsteering using dispersive deflectors and wavelength tuning," Opt. Express **16**, 14617–14628 (2008).
36. H. Gevorgyan, K. A. Qubaisi, M. S. Dahlem, and A. Khilo, "Silicon photonic time-wavelength pulse interleaver for photonic analog-to-digital converters," Opt. Express **24**, 13489–13499 (2016).
37. M. Cherchi, S. Ylinen, M. Harjanne, M. Kapulainen, and T. Aalto, "Dramatic size reduction of waveguide bends on a micron-scale silicon photonic platform," Opt. Express **21**, 17814–17823 (2013).
38. H. Zafar, P. Moreira, A. M. Taha, B. Paredes, M. S. Dahlem, and A. Khilo, "Compact silicon TE-pass polarizer using adiabatically-bent fully-etched waveguides," Opt. Express **26**, 31850–31860 (2018).
39. G. H. Song and W. J. Tomlinson, "Fourier analysis and synthesis of adiabatic tapers in integrated optics," J. Opt. Soc. Am. A **9**, 1289–1300 (1992).
40. N. Li, D. Vermeulen, Z. Su, E. S. Magden, M. Xin, N. Singh, A. Ruocco, J. Notaros, C. V. Poulton, E. Timurdogan, and C. Baiocco, "Monolithically integrated erbium-doped tunable laser on a CMOS-compatible silicon photonics platform," Opt. Express **26**, 16200–16211 (2018).
41. M. T. Wade, F. Pavanello, R. Kumar, C. M. Gentry, A. Atabaki, R. Ram, V. Stojanović, and M. A. Popović, "75% efficient wide bandwidth grating couplers in a 45 nm microelectronics CMOS process," in *Optical Interconnects Conference (OI)* (IEEE, 2015), pp. 46–47.